TÜBİTAK

Turkish Journal of Earth Sciences

http://journals.tubitak.gov.tr/earth/

Research Article

Turkish J Earth Sci
(2017) 26: 127-146

doi:10.3906/yer-1606-7

Depositional stages of the Eğribucak inner basin (terrestrial to marine evaporite and carbonate) from the Sivas Basin (Central Anatolia, Turkey)

Özgen KANGAL[1,*], Nazire ÖZGEN ERDEM[1], Baki Erdoğan VAROL[2]
[1]Department of Geological Engineering, Cumhuriyet University, Sivas, Turkey
[2]Department of Geological Engineering, Ankara University, Ankara, Turkey

Received: 10.06.2016 • **Accepted/Published Online:** 30.09.2016 • **Final Version:** 15.06.2017

Abstract: The Sivas Cenozoic Basin and coeval Central Anatolian basins such as Çankırı and Tuz Gölü are characterized by both marine and terrestrial sediments ranging in age from the Eocene to early Miocene. The evaporite regime here generally appeared during the late stage of Eocene transgression and persisted through the Oligocene time. However, marine-induced Oligocene evaporites are less known because of less paleontological evidence and regional tectonics and salt diapirism that mostly caused the destruction of their original stratigraphic positions. The Eğribucak area studied here, located about 25 km southeast of Sivas**,** provides a well-stratified key section to shed light on the depositional history of the Oligocene marine evaporite (coastal lagoon or sabkha complex) and other associated carbonate and siliciclastic units. The Eğribucak succession has a thickness of approximately 400 m and rests on thick fluviatile sediments commencing with red beds (mudstone, sandstone, and gravelly sandstone), and upwards, terrestrial gypsums are present within the red units as thin beds that are overlain by thick marine gypsum beds with rhythmical alternations of gray and green colored sandstone-marly limestone and limestone. The limestones alternating with the thick gypsum beds are rich in benthic foraminifers yielding a Rupelian-Chattian age. At the top of the section evaporites disappeared and lagoon-type limestone turned into thick platform carbonate dated as Oligocene-early Miocene. The Eğribucak succession shows a wide variety of depositional environments ranging from terrestrial to restricted marine to open marine from bottom to top. The short periods of the lithological alternations from siliciclastic to carbonate and evaporite indicate that the evaporite environment was not consistent through the Oligocene period. This would be formed as a marginal evaporite environment, presumably a coastal lagoon/sabkha affected by seasonal variations with arid and humid periods as well as eustatic sea-level changes. The Oligocene transgression culminated in the area with the deposition of platform-type carbonates and it continued during the early Miocene.

Key words: Terrestrial-marine transition, siliciclastic-carbonate-evaporite transitions, Oligocene evaporites, Eğribucak section, Sivas Basin

1. Introduction

The development of Central Anatolian Cenozoic basins such as Sivas, Çankırı, and Tuz Gölü was related to a series of geological processes that occurred after the closure of the northern branch of the Neo-Tethyan Ocean (Şengör and Yılmaz, 1981; Dirik et al., 1999) (Figure 1). An assemblage of ophiolite mélange related to the İzmir-Ankara-Erzincan suture zone crops widely out in eastern and northeastern parts of the basin (Tatar, 1982; Cater et al., 1991). The Sivas Cenozoic Basin is located on three crucial continental plates. These are the Central Anatolian massif in the west, Pontide Thrust Belt in the north, and Tauride-Anatolian Block in the south. On the other hand, older geological units are exposed in the southern part of the basin. They belong to the suture zone of the Inner Tauride Ocean, which was opening and closing between the Jurassic and the Cretaceous/Paleocene periods (Oktay, 1982; Görür et al., 1984; Tekeli et al., 1992). Since the geological structure of the Sivas Basin is so interesting, many researchers have carried out multidisciplinary studies on the basin (Stchepinsky, 1939; Nebert, 1956; Kurtman, 1961, 1973; Baykal and Erentöz, 1966; Artan and Sestini, 1971; Yılmaz, 1981; Gökten, 1983; Gökçen and Kelling, 1985; Gökçe and Ceyhan, 1988; Aktimur et al., 1990; Cater et al., 1991; Gökten, 1993; Guezou et al., 1996; Poisson et al., 1996; Temiz, 1996; Sümengen et al., 1990; Tekeli et al., 1992; Poisson et al., 1996; Dirik et al., 1999; Ocakoğlu, 2001; Tekin et al., 2002; Gündoğan at al., 2005; Yılmaz and Yılmaz, 2006, Callot et al., 2014, Ribes et al., 2015). The Eğribucak succession studied here constitutes the direct subject of several studies. In particular the sedimentary, stratigraphic, and paleontological features of

* Correspondence: okangal@cumhuriyet.edu.tr

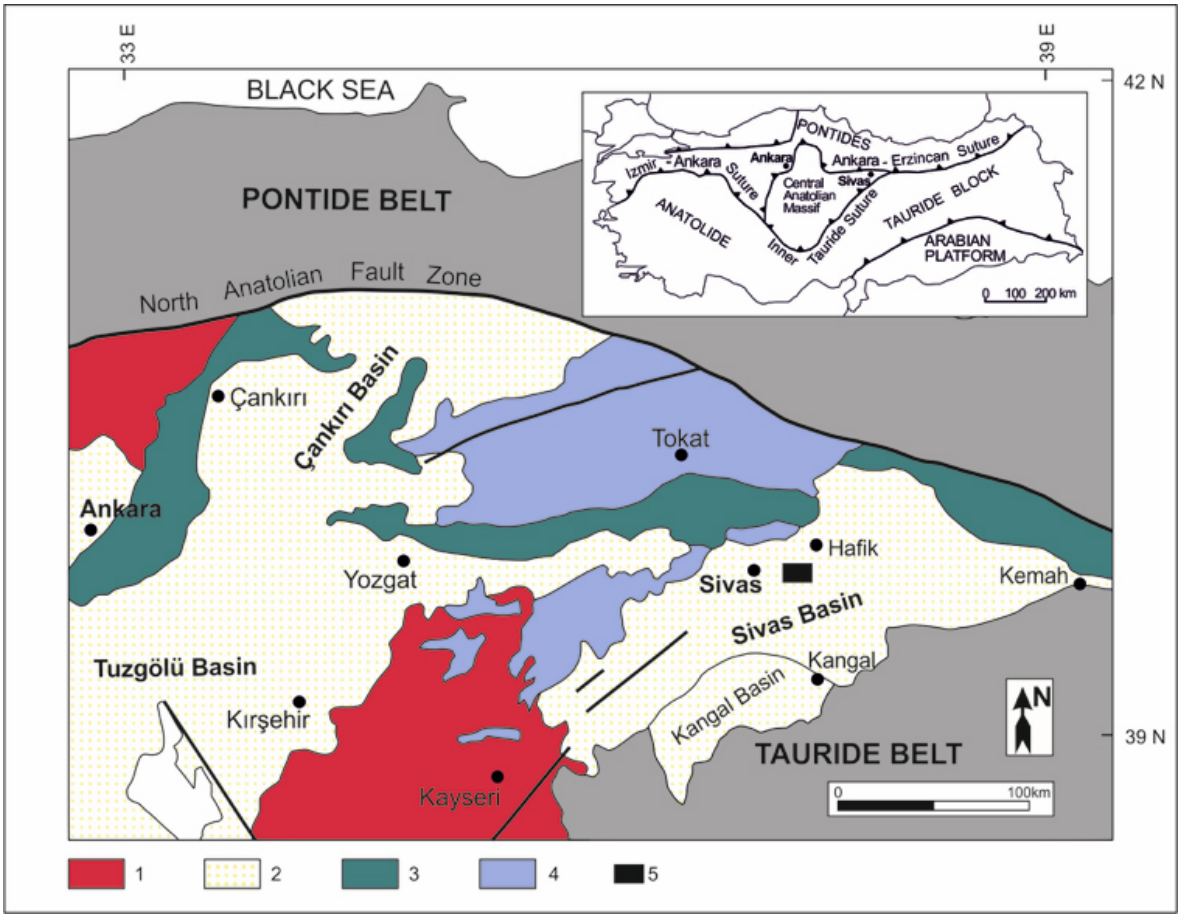

Figure 1. Geological position of the Sivas Basin (geological map modified from Bingöl (1989); tectonic map simplified from Okay and Tüysüz (1999)). 1. Volcanic complex: volcanics and pyroclastics (Miocene-Pliocene). 2. Sedimentary basins (Cenozoic). 3. Ophiolitic mélange (Cretaceous). 4. Metamorphic massifs. 5. Study area.

the succession were mentioned in many studies (Çiner and Koşun, 1996; Çubuk and İnan, 1998; Kangal and Varol, 1999; Çiner et al., 2002; Sirel et al., 2013; Poisson et al., 2015; Hakyemez et al., 2016).

The Sivas Cenozoic Basin underwent the first major regression during the late Lutetian (middle Eocene) that caused uplift of the basin margin and environmental shallowing leading to precipitation of marine evaporite in the local basins through the late Eocene. These hydrological and tectonic events prevailed in the onset of the first evaporite stage through the late Eocene-early Oligocene (Figure 2). The late Eocene evaporites were interrupted by Oligocene thick terrestrial deposits with minor evaporite levels. The evaporite-bearing fluviatile deposits prevail over the western part of the Sivas Basin, particularly present around the Akkışla and Küçüktuzhisar regions. The center and eastern parts of the Sivas Basin remained as restricted shallow marine and precipitated the different kinds of evaporite beds during the Oligocene (Kangal et al., 2005).

This study is focused on the Eğribucak area, which is located 25 km southeast of Sivas (Figures 1 and 3). The study area is represented by one of the best outcrops, which includes tripartite successions such as evaporite, carbonate, and siliciclastic through the Oligocene-early Miocene as marine and nonmarine depositional environments. In the Sivas Basin, the Eğribucak region provides distinctive outcrops to carry out facies analyses and environmental interpretations that clarify the evolution of the evaporite and nonevaporite deposition ranging from the Oligocene to early Miocene. Facies analyses have been conducted on one measured section and obtained results were used to apprise the environmental changes from evaporite-carbonate to siliciclastic and to reveal climatic, tectonic, and eustatic changes during evaporite and nonevaporite depositional events in the Eğribucak inner basin.

2. Methods

Field studies were started with a 400-m-thick measured stratigraphic section, which represented all depositional

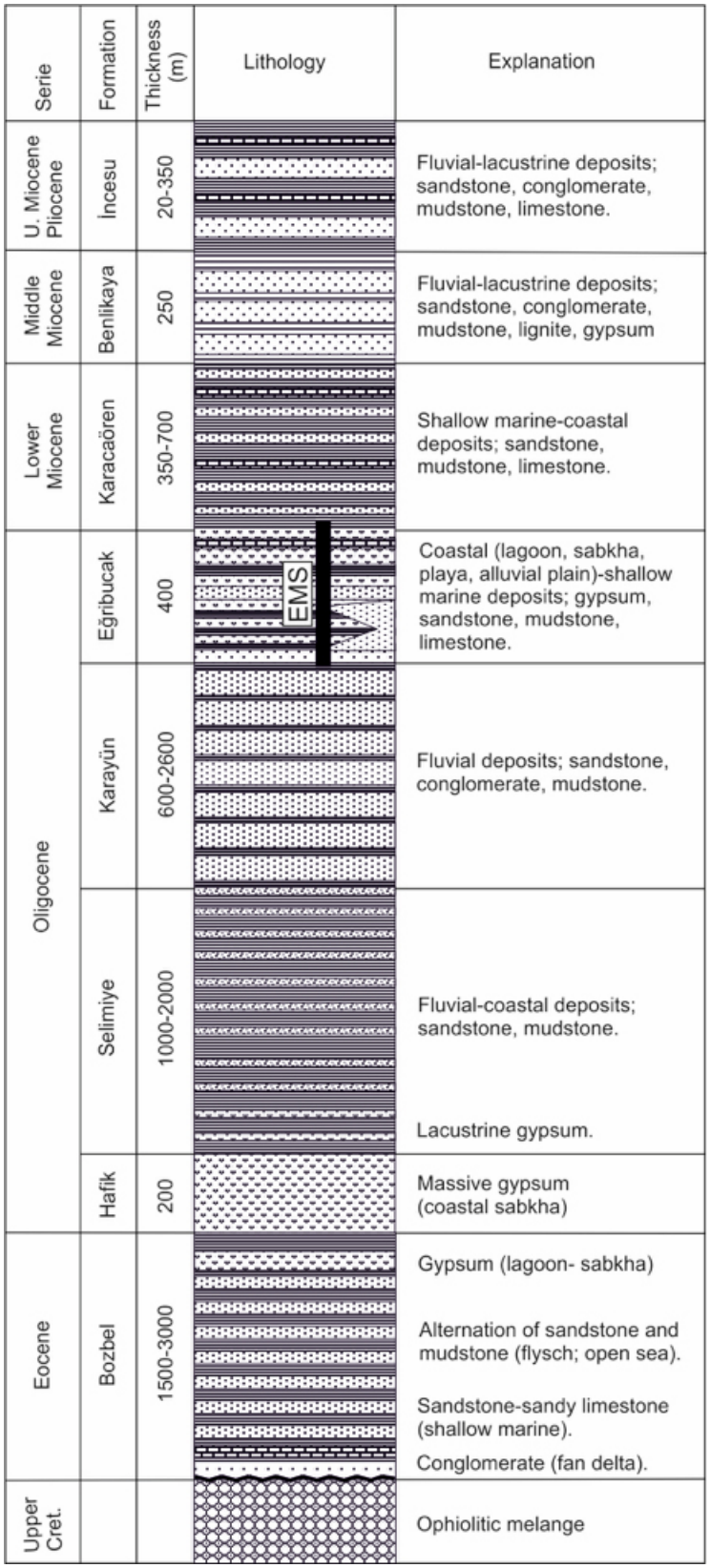

Figure 2. Generalized stratigraphical columnar section of the central and eastern parts of the Sivas Basin (not to scale). EMS: position of the Eğribucak section.

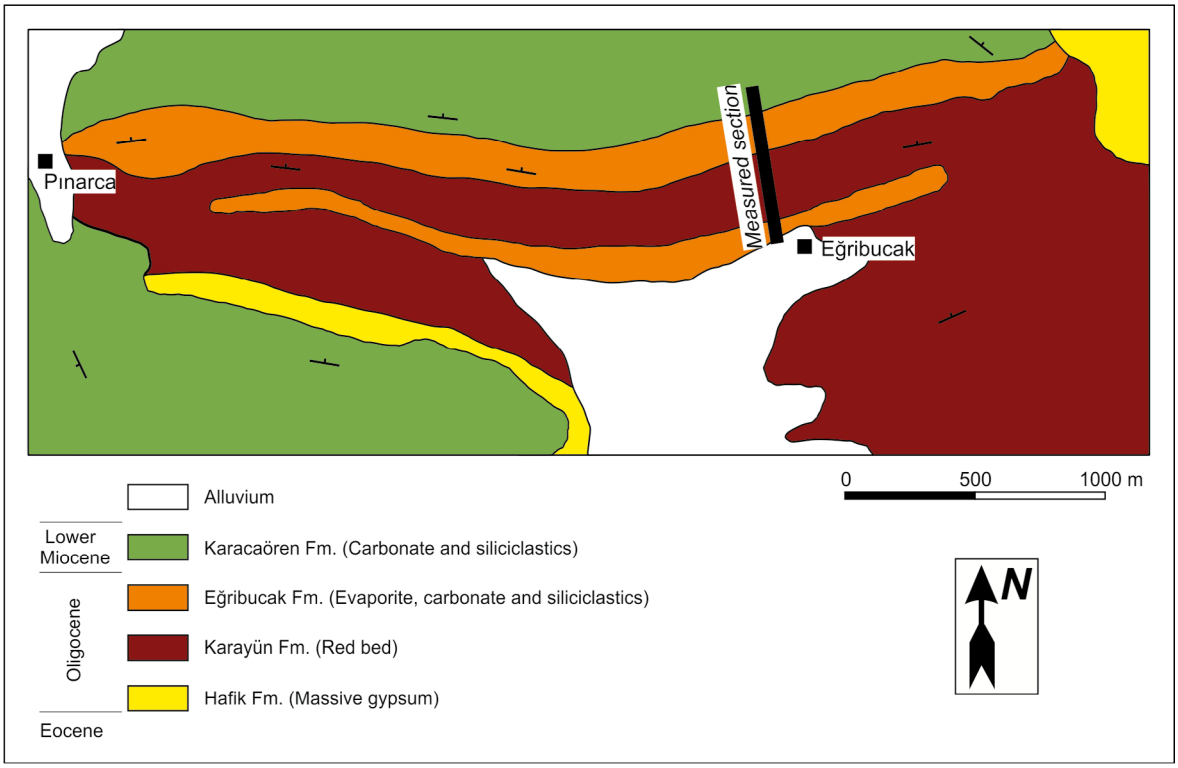

Figure 3. Geological map of the Eğribucak region.

intervals of the Oligocene-early Miocene sequence of some 3000 m in thickness. A total of 120 samples were collected (20 evaporites, 65 carbonates, and 35 siliciclastics). Facies analysis was separately applied to siliciclastic, evaporite, and carbonate units on the basis of lithological and petrographic descriptions. Carbonate rocks were defined with the help of the classifications of Folk (1959, 1962) and Dunham (1962), and their environmental characteristics were interpreted as facies belts and standard microfacies with respect to the models of Wilson (1975). Siliciclastic facies was established by compositional, structural, and textural features such as bedding characters (thin, moderate, and thick/massive beds) and sorting and sedimentary structures (parallel and cross-bedding, current- and wave-induced structures, and biogenic ones, particularly trace fossils).

Evaporite petrography was carried out using an optical polarized light Leica microscope. Thin sections were prepared in the laboratory of the Geological Engineering Department of Dokuz Eylül University, İzmir. The evaporite samples were fixed with polyester in a 50 mm × 50 mm box, which was cut with a diamond saw using an oil system. The slabs were then abraded and polished with water emery paper (80–1200 Atlas mark) using fine machine oil. The polished slabs were cleaned with alcohol and stuck on a slide using Loctite 358 under ultraviolet light. The slabs were thinned until they reached a thickness of about 30 µm. Finally, the thin sections were cleaned with alcohol and covered. The obtained petrographic data help to understand evaporite diagenesis as well as the paleoenvironment of the evaporites.

The petrographic studies are based on a number of interpretations of the evaporite samples such as present evaporite lithology, host-sediment (matrix) and/or nonevaporitic clastic components, secondary gypsum (including cementing satin-spar veins), anhydrite environment-origin (early and late diagenesis), gypsification environment "final exhumation", and original evaporite lithofacies (in the secondary gypsum samples). Geochemical studies were performed as stabile isotopic analyses for carbonate and evaporite rocks. All isotope measurements were conducted in the Geochemistry and Isotope Laboratory of the University of Arizona, USA. Limestones were tested by isotopes of $^{18}O/^{16}O$ and $^{12}C/^{13}C$ from five samples. Results were used to interpret marine water salinity and organic contribution during carbonate precipitation and diagenesis. Similarly, different types of five evaporite samples were subjected to isotopic analyses of $^{86}Sr/^{87}Sr$ and ^{37}S indicating the origin and age of the studied evaporites (Palmer et al., 2004).

3. Geologic setting and stratigraphy

The investigated area, which is 25 km from the city of Sivas to the southeast, is located in the central-eastern part of the

Sivas Basin between Eğribucak and Pınarca villages (Figure 3). In this area, Cenozoic units commenced with massive gypsum formed as a transitional level from the Eocene to Oligocene (Hafik Formation: Kurtman, 1973) and upward, it grades into Oligocene sediments displaying lateral and vertical facies changes and different environmental conditions. The study area is considered as the Eğribucak inner basin (sensu stricto mini basin: Ringenbach et al., 2013; Callot et al., 2014; Poisson et al., 2015; Ribes et al., 2015) because of limited extension of lithological units and an isolated character from the neighboring depositional systems within the Sivas Basin. The evaporites exposed in the Eğribucak succession have been determined in various environments attributed to different ages ranging from early Miocene to middle Miocene (Table 1). A more recent study revealed that the evaporite is Oligocene in age according to foraminifera assemblages within the limestone alternations (Sirel et al., 2013). On the other hand, the evaporite deposition was not only terrestrial in origin, but also it was commonly precipitated under marine conditions (Kangal and Varol, 1999). The Eğribucak succession needs to be revised according to these new paleontological and sedimentologic constraints. In particular, new paleontological findings presented by Sirel et al. (2013) have been useful for this study to explain the time span of the evaporite precipitation in the Eğribucak inner basin. Former studies reported that the Karayün Formation starts with Oligocene-aged basal fluvial deposits, which is equivalent to the Eğribucak Formation's red beds. In this study, the age of the formation was revised as Rupelian-Chattian with respect to determination of new benthic foraminiferal associations (Sirel et al., 2013). This paleontological finding quite differs from the previous studies considering the age of the formation as early-middle Miocene (Çiner and Koşun, 1996; Çiner et al., 2002). The marine limestones and mudstones existing at the top of the Eğribucak succession are included in the Karacaören Formation (Kurtman, 1973) deposited in the Chattian-Aquitanian transition.

4. Sedimentology

The Eğribucak succession was divided into four different sedimentary units with respect to their lithological and environmental features (Figures 4 and 5). The first unit with a thickness of 80 m, which rests on the basal fluvial sediments (red beds), consists of gypsum, mudstone, and sandstone beds, displaying sharp or transitional boundaries. Gypsum beds gradually become thinner in the lateral direction and then disappear within the red mudstone. The unit has been defined as arid coastal plain (sabkha-playa)-lagoon deposits. The second unit attaining a thickness of 100 m is entirely represented by reddish siliciclastics deposited in a fluvial environment, composed of alternating beds of sandstone, conglomerate, and mudstone. The third sedimentary unit of 160 m consists of the alternation of sandstone, mudstone, limestone, and gypsum, which are the products of shallow marine-coastal sedimentation. The fourth sedimentary unit is composed of cream-colored limestone, gray and green pelagic mudstone, and sandstone located at the top of the sequences corresponding to the continuous sedimentation from Chattian to early Aquitanian. Age-diagnostic fossils are encountered from the bank-type platform limestones within this level.

In the facies analysis carried out in the context of taking the measured stratigraphic section, five siliciclastic, four carbonate, and five evaporite, in total fourteen facies were distinguished (Table 2). Apart from carbonates, the description of facies was performed according to the structural and textural characteristics that were mainly observed in the field and supported by petrographic studies. Carbonate facies were determined according to deposition textures (Dunham, 1962).

Table 1. Comparison of recent findings to the previously published data for the evaporite-bearing part of the Eğribucak succession.

Study	Age	Formation	Member	Depositional environment
Çubuk, 1994	early Miocene	Karayün	Danışma Tepe	Playa
Çiner and Koşun, 1996	middle Miocene	Eğribucak	Sekitarla and Pınarca	Sabkha-playa to fluvial
Çubuk and İnan, 1998	early Miocene	Karayün	Danışma Tepe	Playa
Kangal and Varol, 1999	early Miocene	Karacaören	-	Coastal sabkha-lagoon
Çiner et al., 2002	early-middle Miocene	Eğribucak	Middle member	Sabkha to fluvial
Sirel et al., 2013	Rupelian - early Chattian	-	-	Lagoon-very shallow marine (for foraminiferal limestone)
Poisson et al., 2015	Oligocene	Eğribucak	-	Fluvial to lacustrine
This study	Rupelian-Chattian	Eğribucak	-	Shallow marine-coastal (lagoon, sabkha, playa, alluvial plain)

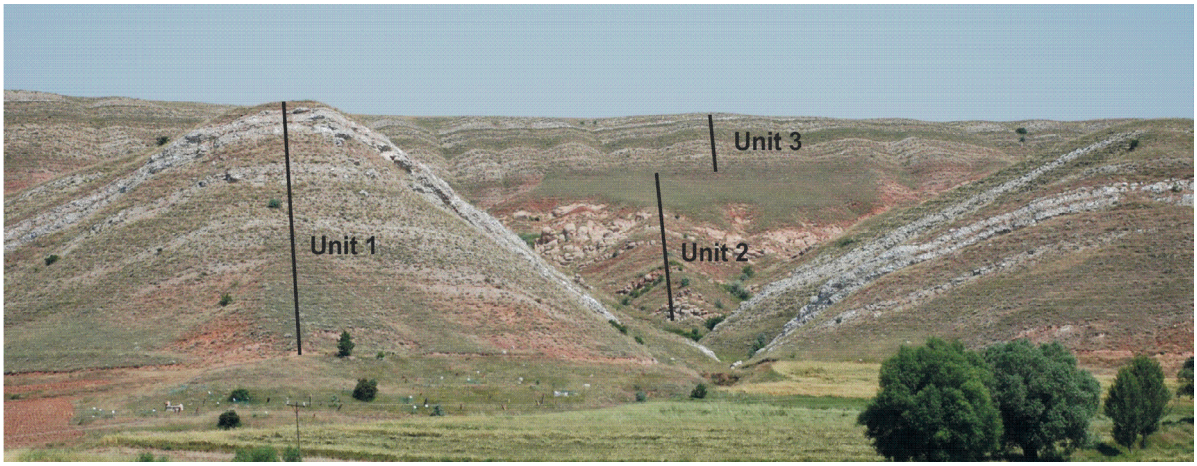

Figure 4. Typical field appearance of the Eğribucak succession and defined sedimentary units.

4.1. Siliciclastic facies

4.1.1. Cross-bedded red sandstone-pebbly sandstone (F1)

This facies is common in the base of the Eğribucak evaporite sequence, formed in the second sedimentary unit with a total thickness of 80 m consisting of alternations of red mudstones (F2) and cross-bedded sandstones-pebbly sandstone. In it, each depositional cycle is of 0.5–5 m in thickness and displays sharp or rarely erosive boundaries. The sandstones have the features of medium to coarse sand size and are moderately sorted with trough and rare planar cross-bedding, parallel and ripple lamination, and cyclic deposition with upward grain size thinning. Fine sand and silt floodplain deposits with moth larval burrows are intercalated with the lag conglomerates and mud intraclasts, which were accumulated in the lensoidal-shaped channels (Figure 6a). Through the upper levels some depositional cycles show amalgamated sandstones with parallel bedding habit, separated by pebbly interlayers including a lenticular or matrix-supported conglomerate composed of subangular and moderately rounded poorly sorted pebbles (0.5–5 cm) that were derived from ophiolite and basal limestones.

Interpretation: The general characteristic of this deposition is fluvial. Sand-fine gravel and locally coarse gravel trough cross-bedding sets mark the middle and upper parts of the lower flow regime (Miall, 1978). This kind of cross-bedding is generally interpreted as the migration products of three-dimensional dunes (Collinson, 1986). The planar cross-bedding observed in this system locally represents the transverse bed loads (Bourquin et al., 2009). The angular-semiangular mud intraclasts in the silty and weakly sorted silty sandstone-sandstone matrix were torn off from mud flats in the base at the flooding stage and transmitted into the channel. In contrast, horizontal stratification, parallel laminars, and bioturbations were formed under low energy conditions (Reineck and Singh, 1980; Miall, 1996). Mainly sand-loading deposition with parallel and cross-bedding characters and weakly developed or largely destroyed flood plain sedimentation mark the deposition of fluvial sand bars and channels in the "sand-bed braided river" system (Bridge and Lunt, 2006).

4.1.2. Red mudstone (F2)

This facies was formed by red and fairly homogeneous mudstones interfingering with the F1. It is widely observed in the fluvial sequence at the base as well as in the first and second sedimentary units. In the first unit the facies contains gypsum layers of variable thicknesses (15 cm on average) with limited lateral extent (10–200 m), whereas it was repetitively channeled by sandstone-conglomerate levels (F1) in the second unit (Figure 6a). Sedimentary structures such as parallel and convolute laminations, root casts, biogenic burrows, desiccation cracks, raindrop impressions, and paleosol are commonly present. The formations of paleosol are in different concentrations at silty and muddy levels deposited around the sandy deposits.

Interpretation: The sediments of this facies were deposited in the flood plain system. Root traces, biogenic burrows, and parallel and convolute laminations reflect the moderate flow regime and relatively fast deposition conditions (Jones and Hajek, 2007). The development of the paleosol in these parts is also weak. Paleosol was commonly found in the fine-grained mudstones that developed in the lower flow regime indicating the distal part of the flood plain with fine-grained sheet sandstones. Thin gypsum layers located in the red mudstones are interpreted as evaporite ponds (playa) that developed in the alluvial plain during arid climatic episodes (Warren, 2006; Varol and Atalar, 2016).

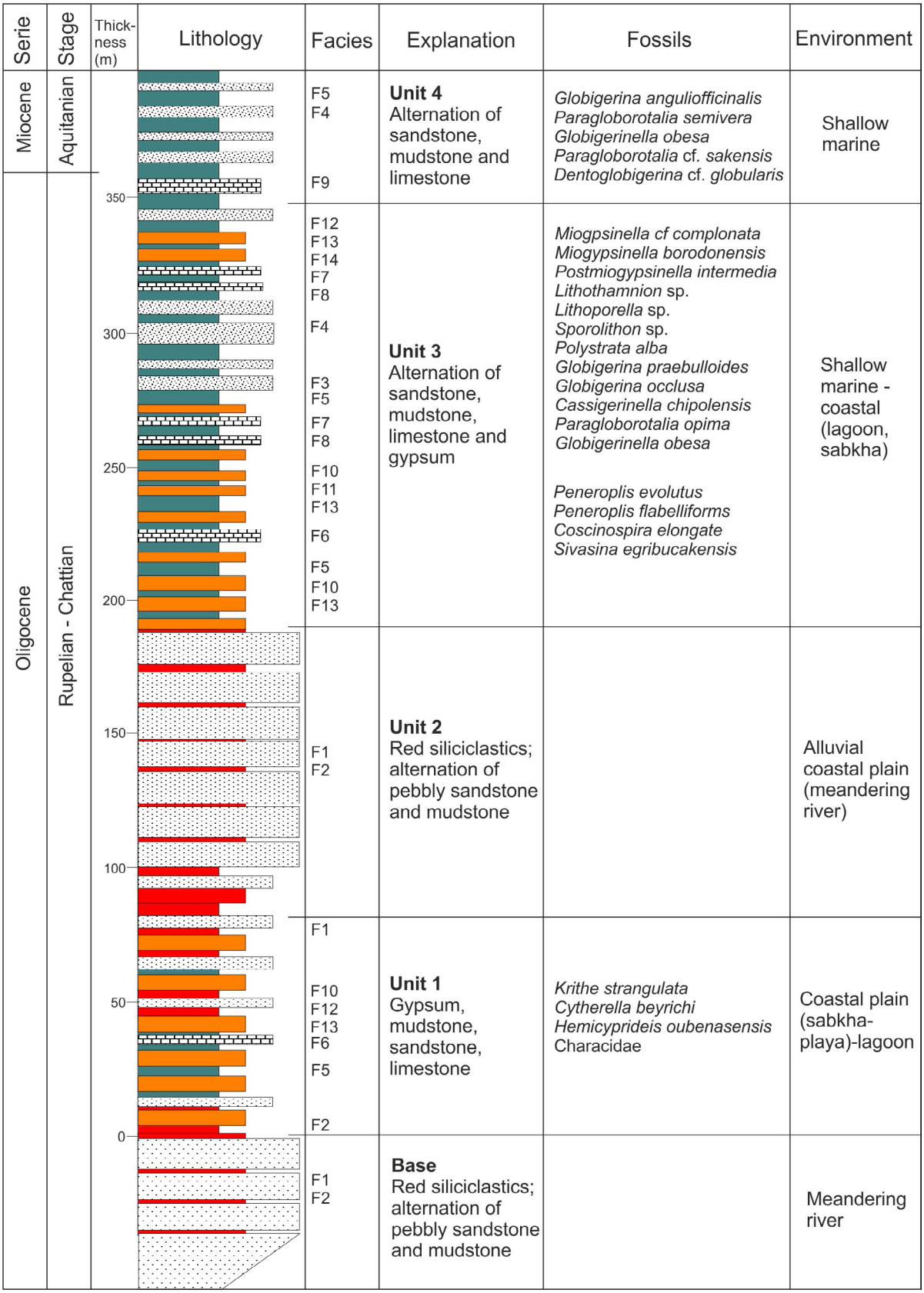

Figure 5. Eğribucak columnar stratigraphic section showing the facies, fossils, and depositional environments.

Table 2. Summary of facies descriptions and their interpretations.

Facies	Description	Comment (environment)
F1. Cross-bedded red sandstone-pebbly sandstone	Red sandstone; with medium-coarse grains, and layer thickness 0.5–5 m; trough and rare planar cross-bedding, gravel levels, mud intraclasts.	Meandering river, channel sediments (Reineck and Singh, 1980; Miall, 1996; Bridge and Lunt, 2006).
F2. Red mudstone	Red massive mudstones; laminated silt-fine sand levels; biogenic burrows, root casts, desiccation cracks, raindrop impressions.	Meandering river, flood plain sediments (Jones and Hajek, 2007).
F3. Cross-bedded calcareous sandstone – pebbly sandstone	Cream-colored pebbly sandstone; poor sorting, planar cross-bedding, fine sand-silt matrix and carbonate cement, channel-fill deposits, broken pelecypod shells, root casts.	Lagoon or bay environment occasionally fed by fluvial systems (Kangal and Varol, 1999; Chaumillon et al., 2008).
F4. Pelecypodal siltstone-sandstone	Lateral continuous siltstone layers (10–30 cm in thickness) and sandstone (lithic arenite) layers (20–50 cm in thickness) within the siltstones; pelecypod shells, carbonized plant fragment, laminations, wave ripples, root cats.	Low-energy coastal marine environments (lagoon and estuary; changing salinity: from brackish to normal marine (Stenzel, 1971; Vermeij, 1972; Ronen, 1980; Reineck and Singh, 1980; Weimer et al., 1982; Varela et al., 2011).
F5. Gray-green mudstone	Gray-green mudstone interbedded with F4 facies; changes silt-clay-carbonate content; average layer thickness is 20 cm; changes in fossil contents (ostracods, charophytes, benthic foraminifers, pelecypods, gastropods, and planktonic foraminifers) at different levels of the succession.	Shallow marine (shore-offshore)-coastal lagoon.
F6. Fossiliferous mudstone	Gray-cream colored, thin-bedded or laminated limestone (rarely dolomite); ostracods, charophytes, and relict plant.	Very shallow marginal marine environment (upper supratidal) intensively subjected to meteoric exposure (Wright and Tucker, 1991; Sherman et al., 1999; Batten Hander and Dix, 2007).
F7. Pelecypodal wackestone-packstone	Creamish-pink thin limestone (10–30 cm thick); micrite matrix; the main components are micrite matrix and pelecypods, to a lesser extent gastropod, ostracod, and benthic foraminifera. Micrograda tion and geopetal structures.	Restricted platform (FZ 8) (Wilson, 1975; Flügel, 2004). Periodically open sea connection (Playford and Cockbain, 1976).
F8. Benthic foraminiferal packstone-grainstone	Sparite cement and micrite matrix at a varying rate;the main component is benthic foraminifera, to a lesser extent algae, bryozoa, and pelecypod shells. Terrigenous quartz grains of silt size; different cementation stages, clothed grains, algal microborings; staining of some shells with iron; umbrella structure is common.	Open platform (FZ 7) (Wilson, 1975; Flügel, 2004).
F9. Algal boundstone	Moderately thick-bedded (30–50 cm thick) and jointed algal limestone; the main component is red algae, also bryozoa and benthic-pelagic foraminifera. Micrite matrix and sparite cement at varying ranges in internal spaces.	Platform margin reef "algal mounds" (FZ 5) and slope (FZ 4) (Wilson, 1975; Flügel, 2004).
F10. Bedded selenite gypsum	Coarse gypsum crystals orientated in the vertical direction; layer thickness is 5–150 cm; some crystals retain original shape; the inside of coarse crystals is filled with microcrystalline gypsum.	Primary underwater (shallow) gypsum; bottom-nucleated upward gypsum growth (Handford, 1991; Warren, 1999, Schreiber and Tabakh, 2000; Paz and Rossetti, 2006).
F11. Laminated gypsum	Gypsum interlaminated with mudstone-carbonate mudstone; alabastrine texture.	Intratidal-intertidal lagoons (Warren and Kendal, 1985; Hanford, 1991; Kendal and Harwood, 1996).
F12. Clastic gypsum (gypsarenite)	Clastic gypsum laminae or beds alternating with siliciclastic material; grading, parallel-cross lamination.	Reworking of evaporite plain gypsum by waves and fluvial processes (Magee, 1991).
F13. Nodular bedded gypsum	White and cream nodular gypsum layers (thickness 1–30 cm); nodules are elongated in the vertical direction and display a semispherical shape. Chicken wire and enterolithic structures, alabastrine-mosaic texture.	Supratidal evaporite plains (sabkha) (Testa and Lugli, 2000).
F14. Single selenite gypsum crystals	Prismatic-twinning single gypsum crystals scattered in mudstone.	Gypsum-saturated pore water in mud flats (Cody and Cody, 1988; Rosen and Warren, 1990; Magee, 1991).

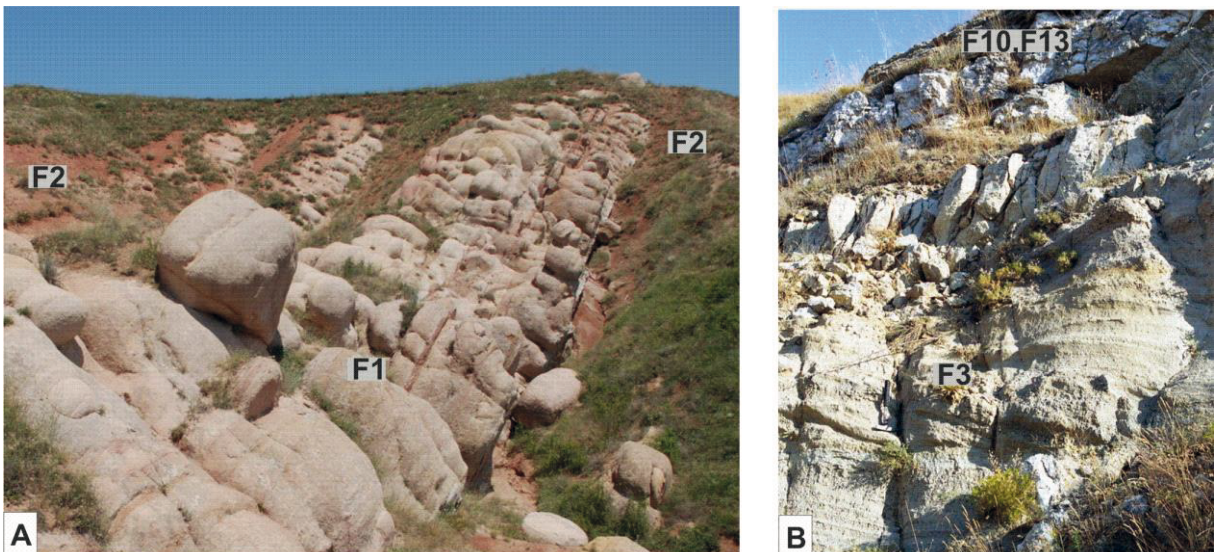

Figure 6. a) Field photo showing the alternation of cross-bedded red sandstone-pebbly sandstone (F1) and red mudstone (F2) facies. b) Field photo showing the transition of cross-bedded carbonated sandstone-pebbly sandstone (F3) and evaporite facies (F10, F13).

4.1.3. Cross-bedded calcareous sandstone-pebbly sandstone (F3)

This facies is observed in a limited part of the third unit, characterized by evaporite, carbonate, and siliciclastic transitions of the succession, formed from cream-colored, planar cross-bedded, and poorly sorted pebbly sandstone. The root casts take place in the muddy levels resting on the evaporites (gypsum). Fragments of pelecypod shells are also found in the facies with an abundant carbonate content. The facies providing lenticular geometry in gray-green mudstone (F5) reaches to 2 m in thickness and upward grades into the pelecypod-bearing sandstone (F4) (Figure 6b).

Interpretation: The sediments of this facies were deposited in the first stage of the marine input terminating terrestrial sedimentation. In particular, channel-fill deposits represented by cross-bedded pebbly sandstones are the typical examples of incised valleys developing in front of the progressing coastline (Chaumillon et al., 2008). The levels with evaporite transition indicate the restricted water circulation/closed environmental conditions together with climatic changes displaying short-term aridifications. This sedimentation type might have partially taken place in a bay or lagoon environment occasionally fed by fluvial systems and periodically undergoing climatic processes with intense evaporation (Kangal and Varol, 1999).

4.1.4. Pelecypodal siltstone-sandstone (F4)

This facies is represented by predominantly siltstone and fine- to medium-grained sandstones that are locally and typically observed at the upper part of the sequence (third and fourth sedimentary unit). Siltstones consist of lateral continuous layers of 10–30 cm in thickness and can reach thicknesses of 10–15 m in total. The concentration of the material of ophiolite origin is clear in the sandstones forming distinctive layers of 20–50 cm in thickness within the siltstones. Carbonized fragments of plants are common in siltstones, and they are observed in the form of thin lignite layer-lamina from place to place. The main sedimentary structures observed in the facies are laminations, wave ripples, and the traces of root casts. Pelecypod shells (especially ostreid) in this facies are mainly observed as clusters but rarely fractured.

Interpretation: The sediments of this facies were deposited in wide environmental conditions ranging from sea to brackish water. Constituting the primary fossil assemblage of the facies, ostreids are forms that adapt well to low-energy coastal marine environments (lagoon and estuary) with changing salinity of the water (from brackish to normal marine) and forming colonies clinging to the ground (Stenzel, 1971; Kirby, 2000; El-Hedeny, 2005). Lignite levels with pelecypods reflect the coastal and marshy conditions with restricted water circulation (Vermeij, 1972). On the other hand, lensoidal-shaped accumulations of the broken shell (pelecypod) fragments accumulated as coquinas and bioclastic sands with gradations and laminations indicate that storm activity periodically occurred in the lagoon or the lagoon-bounded shallow marine bar represented by a transitional character ranging from marine to brackish environment deposited both siliciclastics and carbonates (Reineck and Singh, 1980; Ronen, 1980; Weimer et al., 1982; Varela et al., 2011).

4.1.5. Gray-green mudstone (F5)

This facies is one of the most widespread facies in the Eğribucak sequence. Depending on the proportional change in clay, silt, and carbonate components, it shows lithological alternations (siltstone-mudstone-marl). It is also one of the richest facies of the sequence in terms of fossil diversity.

Its thickness varies between 10 and 30 cm and it makes up lateral and vertical transitions with the red mudstone and gypsum of the first unit. The layers include some ostracods (*Krithe strangulata* Deltel, *Cytherella beyrichi* (Reuss), *Hemicyprideis oubenasensis* Apostelescu, and *Hemicyprideis* sp.) and undetermined charophytes (Tunoğlu et al., 2013). The mudstones upward grade into the third unit and comprise benthic foraminifers (particularly peneroplid and miliolid forms) accompanied by pelecypods and gastropods. Some layers also include various amounts of planktonic foraminifera such as *Globigerina*, *Paragloborotalia*, and *Globorotaloides*. Individual selenite crystals appear in the mudstone of the third unit.

Interpretation: The sediments of this facies were accumulated under different paleoenvironments ranging from marine (shore – offshore) to brackish (coastal lagoon), which are supported by the facies-bound fossils. Brackish water fauna characterized by ostracods and charophytes is seen in the lower part of the section (unit 1). The distribution of fossils encountered from this facies indicate that the sea level gradually increased in time, leading to the drastic environmental changes from restricted marine/brackish water to normal marine shore/offshore through the Oligocene.

4.2. Carbonate facies

In the Eğribucak sequence, carbonate facies were deposited in different environments, so it displays vertical and lateral transitions to siliciclastic to evaporite environments. Four different types of carbonate facies can be identified based on the microscopic properties, in particular considering their fossil content and textural characteristics.

4.2.1. Fossiliferous mudstone (F6)

This facies comprises thin-bedded (several centimeters thick) or laminated limestones (rarely dolomite) interbedded with gypsum beds within the first and third sedimentary units. Abundance and diversification of fauna and flora is very low and represented by mainly ostracods, charophytes, and relict plants. Noncarbonate grains are silt-sized quartz, volumetrically less than 10%. The facies is described as fossiliferous wackestone according to Dunham's (1962) carbonate rock classification (Figure 7a).

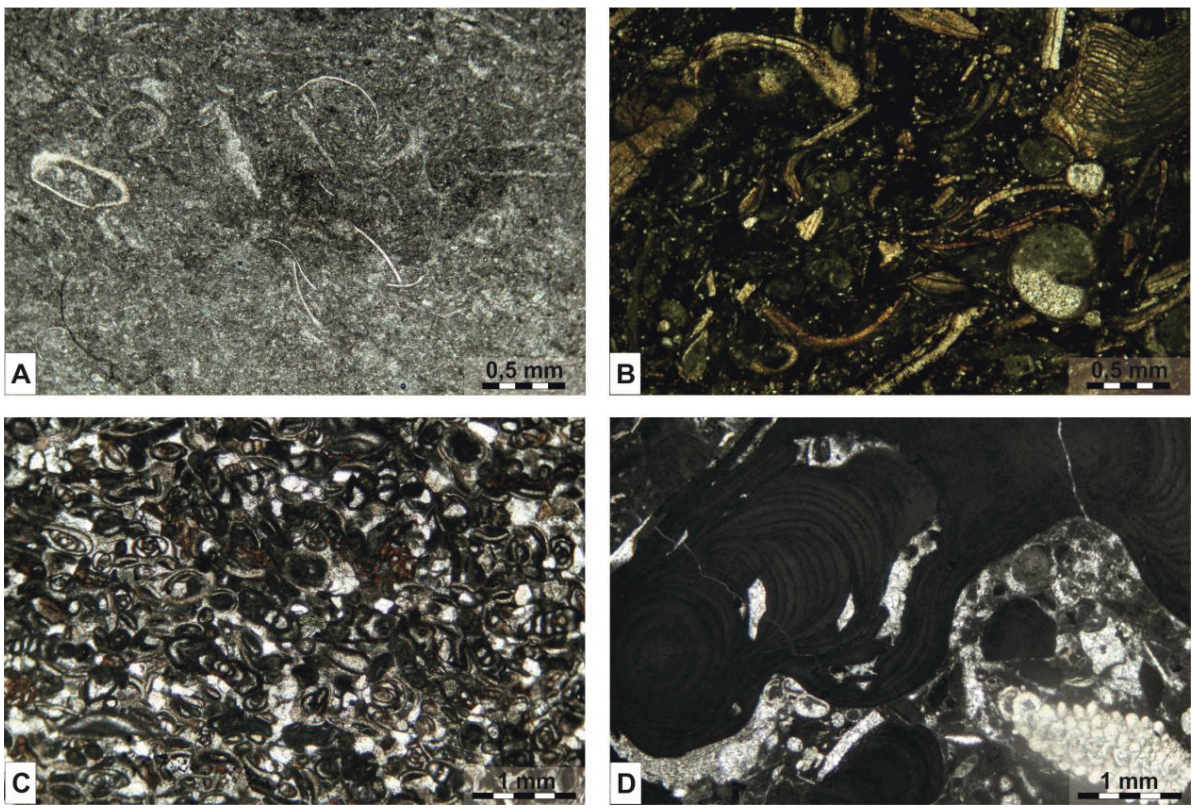

Figure 7. Carbonate facies types (thin section): a) fossiliferous mudstone (F6), b) biogenic–shelly wackestone (F7), c) benthic foraminiferal packstone-grainstone (F8), d) algal boundstone (F9).

Interpretation: The facies has been ascribed to a brackish water environment responding to fossil content (ostracods and charophytes) and also plant material reflects a very shallow marginal marine environment (upper supratidal) intensively subjected to meteoric exposure indicated by meniscus cements, neomorphism, and dissolution (Wright and Tucker, 1991; Sherman et al., 1999; Batten Hander and Dix, 2007).

4.2.2. Pelecypodal wackestone-packstone (F7)

The facies occurs as creamish-pink thin limestone (10–30 cm thick) within the evaporite and red-mudstone succession of the third sedimentary unit. Main components of this facies are the micrite matrix and pelecypods in varying proportions. In different samples a few gastropods, benthic foraminifera (mainly miliolid and peneroplid), and ostracod fossils are encountered. On the other hand, microgradation and geopetal structures are typical sedimentary features of this facies (Figure 7b).

Interpretation: Although the facies is generally a result of low energy conditions, muddy and shelly laminae, microgradation and geopetal structure, and silt-sized internal carbonate sediments indicate that short-period storm and/or tidal activities prevailed that ended the environmental quiescence (Playford and Cockbain, 1976). The facies attributes are consistent with the environment of an estuarine or restricted coast, temporally affected by storms, presumably generated from driven tides (Filgueira et al., 2014). The facies can be also classified as a restricted platform (FZ 8) (Wilson, 1975; Flügel, 2004) that is periodically an open sea connection.

4.2.3. Benthic foraminiferal packstone-grainstone (F8)

This facies is observed in the third sedimentary unit and characterized by spar and poorly washed spar cements with various amounts of micrite and micritic intraclasts accompanied with whole or fragmented biogenic materials derived from different kinds of micro- and macrofossils such as benthic foraminifera (miliolid and peneroplid), pelecypods, red algae and bryozoans (Figure 7c). Terrigenous grains (dominantly quartz) are volumetrically 10%, occasionally up to 25%, accompanied with the rock composition. In some parts, three phases of cementing were precipitated, initially micrite cement around the carbonate grains followed by dog-tooth and blocky spar cements towards the vug center. On the other hand, carbonate grains, mostly pelecypods, were rimmed by irregular micrite coatings in resemblance of superficial ooids (Calner and Eriksson, 2012). An umbrella structure that developed in the shelter area of pelecypods and FeO replacement in the fossil's walls and coatings of unlaminated dark micrite, which rounds off the biogenic particles, mostly pelecypod shells, are common sedimentary features.

Interpretation: Faunal diversity and common components of biogenic grains suggest that an open platform environment existed during the deposition of this facies. Carbonate mud was widely winnowed by tidal currents or tidal-driven storms leading to well-developed porosity between carbonate grains, occupied by micrite, scalenohedral dog-tooth, and equant druzy ferroan spar cements, respectively. These cementing phases indicate that fresh-water influx into the marine environment invoked the pervasive precipitation of dog-tooth sparry calcite cement upon the micrite cement, resulted from decreasing Mg ions during early diagenesis, and they were finalized by ferroan calcite spar cement precipitated under late diagenetic conditions (Flügel, 2004). Siliciclastic and FeO-rich grains (olivine, augite) were transported from ophiolitic terrane to a marginal marine environment during the fresh-water influx. Micrite was consistently removed as a result of the winnowing via storm or tidal activities, and it only remained in sheltered areas under the pelecypod shell "umbrella structure" (Bartholdy and Aagaard, 2001) and internal voids. Coated grains appear as thin irregular micritization zones around the pelecypods that resulted from the alteration of original skeletal grain fabric to a cryptocrystalline texture by repeated algal microborings and subsequent filling of the microborings by micritic precipitates (Bathurst, 1966; Reading, 2000). The environmental attributes are generally consistent with an open platform environment (FZ 7) (Wilson, 1975; Flügel, 2004) that was presumably a high and low energy tidal flat environment dissected by tidal channel bioclasts, coated grains, and intraclasts.

4.2.4. Algal boundstone (F9)

The facies present in the upper part of the third sedimentary unit makes up a lateral transition with the gray-green mudstone facies (F5). Moderately thick-bedded (30–50 cm thick) and jointed algal limestone is the prevailing lithology, cumulatively up to a thickness of 10–15 m. Red algae species are very common, represented by algal knolls/mounds of *Polystrata alba* (Pfender), *Sporolithon* sp., *Lithoporella* sp., and Acervulinidae. In situ growth of algal boundstone and beds composed of algae-derived bioclasts, red algal nodules, bryozoans, benthic foraminifera (mostly Miogypsinidae), and varying rates (5%–15%) of pelagic foraminifera (*Globigerina praebulloides* Blow, *Globigerina occlusa* Blow & Banner, *Globigerina ouachitaensis* Howe & Wallace, *Globigerina gnaucki* Blow & Banner, *Cassigerinella chipolensis* (Cushman & Ponton), *Paragloborotalia opima* (Bolli), and *Globigerinella obesa* (Bolli)) have been identified within the facies (Özgen-Erdem et al., 2013; Hakyemez et al., 2016). In the boundstone, shelter-type porosity was well developed, which constrains the reservoir character of these rocks. Micrite-size carbonate grains probably were derived by erosion of the algal material and filled the interior vugs together with spar cement that formed a geopetal structure with reduced porosity (Figure 7d).

Interpretation: The facies indicates that a high energy environment provided suitable conditions for the red algal colonization formed as knolls/mounds showing crustose to protuberant growth form (Wienberger and Friedlander, 2000) and in some places individual algal nodules (rhodolites: Bosence, 1983) flourished down the hard surfaces. The protuberant structure points out a platform margin setting connected with open marine water leading to transportation of pelagic fauna into the algal colonization. According to the data, the facies could be considered as facies zones FZ 5 (platform margin reefs) "algal mounds" and FZ 4 (slope) (Wilson, 1975; Flügel, 2004).

4.3. Evaporite facies

The parameters used in the facies definition of evaporate rocks are based on the crystallization feature, texture, diagenesis, and formation processes in accordance with the study purpose. We have utilized the same basic facies terminology established by Schreiber et al. (1976) and Babel (1999). These are: a) crystal growth attached to the base (selenite layers), b) chemical deposition (fine-grained bedded or laminated gypsum), c) clastic gypsum (bedded-laminated gypsarenite/rudite), d) diagenetic nodular-bedded gypsum (alabastrine), and e) single selenites. With this perspective, five evaporite facies, bedded selenite gypsum (F10), laminated gypsum (F11), clastic gypsum (F12), nodular bedded gypsum (F13), and single selenite gypsum crystals (F14), have been distinguished in the Eğribucak succession.

4.3.1. Bedded selenite gypsum (F10)

The facies is the most common evaporite formation in the Eğribucak sequence, represented by white and cream coarse gypsum (selenite) crystals lined up in the vertical direction, the crystal size of which can reach a few centimeters (Figures 8a and 8b). The bedded selenite is between 5 and 150 cm thick and it can be laterally deduced 3 km in the inner basin. In some places gray and green mudstone (F5) with a thickness of several meters and limestone (30–50 cm thick) are present within the evaporite facies. In the petrographic analyses, it was detected that bedded gypsum facies (F10, F11, and F13) were represented by "alabastrine" secondary gypsum containing mainly abundant anhydrite inclusions (Figure 8d). In addition to this, textural characteristics show some differentiations such as large porphyroblastic and granoblastic gypsum along with satin spar and alabastrine gypsum matrix.

Interpretation: The development of the facies in the form of the gradual growth of radial gypsum crystals outwards reflects the stages of periodic desiccation and flooding in the shallow marine evaporite environment or brine pan (Babel, 2005; Peryt, 2008). These vertically orientated large crystals developed underwater (shallow water) with upward and radial growth patterns from the sedimentary base and are interpreted as the primary gypsum formations, but then altered to secondary gypsum. Recrystallization of hydration gypsum leads to unequigranular granoblastic gypsum, in unstrained and perfectly oriented grains. Porphyroblastic gypsum may also be a result of recrystallization of the alabastrine variety (Holliday, 1970; Handford, 1991; Warren, 1999; Schreiber and Tabakh, 2000; Paz and Rosetti, 2006).

4.3.2. Laminated gypsum (F11)

This facies that can be rarely distinguished in the Eğribucak sequence has been formed by gypsum laminas interbedded with very fine mudstone-carbonate mudstone laminae and its total thickness can reach just a few centimeters. The facies is underlain by bedded selenite gypsum (F10). Nodular bedded gypsum (F13) is located on the top of the facies (Figure 8b). Enrichments by organic substances are encountered in the form of very thin bituminous mudstone laminae with algal remnants, which are interbedded with laminated gypsum. Carbonate mudstone laminae often have the characteristics of dolomite. In the thin section examinations, it was observed that the gypsum laminae prevalently showed an alabastrine texture (Figure 8d).

Interpretation: Carbonate interlaminae/bands show that evaporite conditions are cut by environmental humidity from time to time, and this reflects the periods of seasonal fluctuations (arid–wet) (Manzi et al., 2009). The sequence with mudstone and carbonate laminae with algal-derived organic contribution of the facies shows that intratidal and intertidal environments were temporarily developed, probably close to evaporite plain precipitated gypsum laminae with the pervasive dolomitization of the carbonate laminae (Warren and Kendal, 1985; Hanford, 1991; Kendal and Harwood, 1996).

4.3.3. Clastic gypsum (gypsarenite) (F12)

This facies consists of clastic gypsum laminae or beds alternating with siliciclastic materials. Clastic gypsum is distinguished in the white and cream-colored portions and is made up of silty-fine sand size components with moderately to poorly developed grain roundness. Nonevaporitic portions are dark gray in color, mainly derived from ophiolite terranes (Figure 8c). Sedimentary structures such as grading, parallel and cross lamination can be selected in this gypsum facies. This facies, reaching approximately 20–30 cm in thickness, has lenticular geometry and it has been encountered in the first and third units of the sequence. In the petrographic examination, an equigranular granoblastic alabastrine texture was deduced, in which some portions show dispersed anhydrite remains and partly distinguished straight grain boundaries.

Interpretation: Clastic gypsum was formed as a result of the reworking of evaporite plain gypsum by waves and fluvial processes (possibly by flooding). It is stated that the facies of this type, especially fine-grained ones, can also develop with

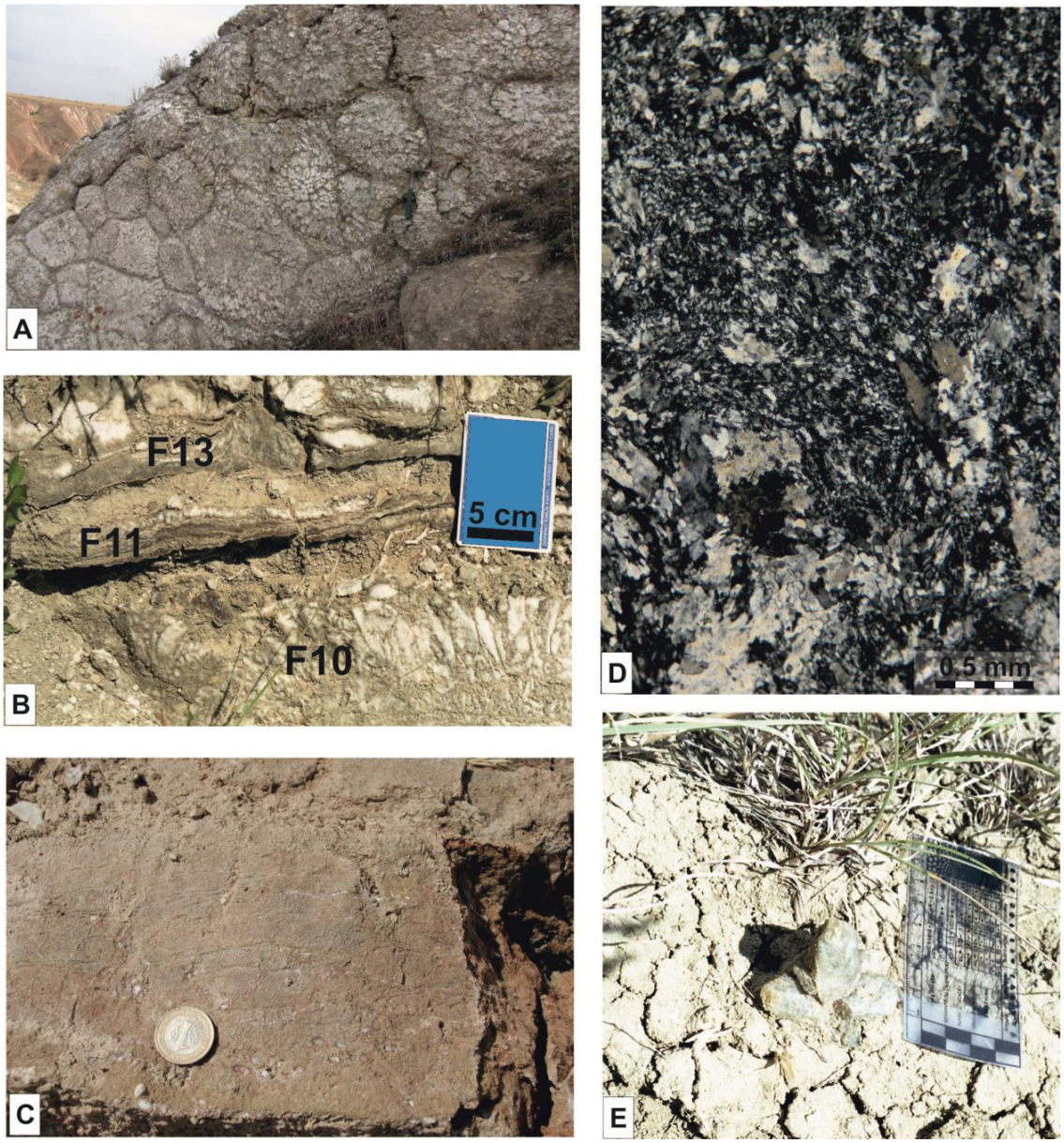

Figure 8. Field photo showing the evaporite facies (except d). a) The stratigrafied gypsum facies (F10 and F13) formed by the growth of coarse gypsum (selenite) crystals in vertical-outward direction. b) Bedded selenite gypsum (F10), laminated gypsum (F11), and nodular bedded gypsum (F13). c) Clastic gypsum (gypsarenite). d) Secondary gypsum texture: "alabastrine" (thin section). e) Single selenite gypsum crystals (F14).

aeolian processes as well as hydrologic processes (Magee, 1991). Our clastic gypsum samples indicate deposition under hydrologic conditions, probably wave activity that involved the sedimentary structure of grading, parallel, and cross lamination within the gypsum facies.

4.3.4. Nodular bedded gypsum (F13)

This facies, represented by white and cream nodular gypsum layers, is observed to be transitive with bedded selenite gypsum (F10) and is often located above it. The nodules in the form of layers with thickness varying from 1–2 cm to 30 cm are elongated in the vertical direction or have a semispherical shape, and their sizes vary from millimetric scale to a few of 10 cm (Figures 8a and 8b). Chicken-wire structures and enterolithic structures and dark lines around the nodules are usual in the facies. In thin sections they show an alabastrine-mosaic texture, in which anhydrite remnants could be identified from place to place (Figure 8d).

Interpretation: These nodules are interpreted as pseudomorphs formed by the dehydration and rehydration of selenite crystals, supported by some relict crystals displaying elongated positions in the vertical direction. This kind of nodular structure can be commonly formed in supratidal evaporite plains during early diagenesis (sabkha) (Testa and Lugli, 2000) or alternatively they originated from the mobilization of sulfate-rich fluids during late diagenesis (burial), probably related to halokinesis (Paz and Rossetti, 2006).

4.3.5. Single selenite gypsum crystals (F14)

This facies is represented by single gypsum crystals observed as being dispersed inside mudstone (F5) and the size of which reaches up to 10 cm (Figure 8e). These crystals offer mostly prismatic but sometimes twinning crystal forms. The facies is observed at a single level in the third sedimentary unit.

Interpretation: This type of evaporite crystals with free growth was formed by the condensation of high evaporite pore water in the mud flat. The development of the crystals is in the displacive form in a mud matrix close to the muddy brine surface (Cody and Cody, 1988; Rosen and Warren, 1990; Magee, 1991). On the other hand, lenticular sand-sized forms, which are similar to those studied herein, make up the uppermost lake sediments and the gypsum lunettes about the salt flat edge of coastal saline flats and continental salt lakes (Warren, 1999).

5. Stable isotope data

5.1. Carbonates

The isotope data considered here are only preliminary results concerning typical carbonate facies of the Eğribucak succession. As shown in Table 3, the samples from benthic foraminiferal packstone-grainstone (F8) and algal boundstone (F9) yield relatively decreasing $\delta^{18/16}O$ isotope values compared with calculated values for Oligo-Miocene marine water ($\delta^{18/16}O$ = –2‰ to +2‰: Reuter et al., 2013) or for Oligocene shallow water ($\delta^{18/16}O$ = –0.5‰ to +1.5‰: Milliman, 1974; Veizer, 1983).

Interpretation: Stabile isotopes $\delta^{18/16}O$ and $\delta^{13/12}C$ provide important parameters to determine environmental, paleogeographic, and paleoclimatic characteristics of the carbonate rocks. In particular, the stable isotopes supply accurate data for the interpretation of the salinity, temperature, and organic activity during carbonate precipitation or diagenesis. As a general context, carbon isotopes are widely used to trace the origin of carbon, while oxygen isotopes store paleotemperature information. On the other hand, isotopic measurements ($\delta^{18/16}O$ and $\delta^{13/12}C$) of the carbonate shells are widely used for considering the evolution of the world's seas concerning their glaciation and postglaciation stages or wide-ranging correlations of the geological units in different parts of the world (Miller et al., 1991; Jacobsen et al., 1999; Mutti et al., 2006; Kakizaki et al., 2013).

Table 3. Isotopic analyses of carbonate samples recovered from the Eğribucak section.

Sample no.	Facies	$^{18/16}C$	$^{13/12}O$
EB1	F9. Algal boundstone	–1.45	–3.00
EB1e	F8. Benthic foraminiferal packstone-grainstone	–1.92	–5.12
EB11	Benthic foraminiferal packstone-grainstone	–1.06	–4.43
EB21a	F8. Benthic foraminiferal packstone-grainstone	0.46	–6.84
ED3	F9. Algal boundstone	–1.54	–3.58

Carbon isotope ($\delta^{13/12}C$) in oceanic marine water is between 1‰ and 2‰ (Hudson, 1977) and also the carbon isotope ratio has been calculated between 1‰ and 4‰ for some shallow water carbonates (Veizer, 1983 according to the diagram of Milliman (1974)). In the Eğribucak carbonates, the carbon isotope value of one sample (Eb21a) falls into the range of normal marine environments. Other samples have slightly negative values relative to the given value for marine carbonate (1‰ to 2‰). Generally, carbonates forming in brackish water have reduced $\delta^{13}C$ values that are in proportion to the degree of fresh water dilution with incorporation of isotopically light CO_2 from land or decomposition of organic matter. In the studied samples, $\delta^{18/16}O$ values fall into two groups: weakly decreasing isotope values (algal boundstone) and strongly decreasing isotope values (benthic foraminiferal packstone-grainstone). In the facies analyses, the first group lies in a normal open marine environment. Thus, fresh water contribution seems to be unlikely for these negative values. It can be linked to temporal uplifting of the algal mounds that invoked the somewhat diagenetic alteration of high-Mg calcite algal shells to low-Mg calcite with light oxygen isotopes (Allan and Matthews, 1982; Reuter et al., 2013), whereas the second group gives an implication of a high rate of fresh-water influx into the shallow and restricted coastal marine environment during precipitation of limestone. The environment can be interpreted as brackish water, being useful for producing the strongly negative $\delta^{18/16}O$ isotope. These isotopic behaviors are biased toward more negative values and can correspond to both diagenesis or freshwater influx and diagenetic alteration of the fossil shells (De Man et al., 2004).

5.2. Evaporites

The results of the stable isotope analysis are taken from four gypsum facies in the Eğribucak succession. They are

bedded selenite gypsum (F10), laminated gypsum (F11), nodular bedded gypsum (F13), and single selenite gypsum crystals (F14), which are given in Table 4.

Interpretation: Evaporites provide limited data to make possible stratigraphic correlations and dating due to scarce fossil content and also they display very complex depositional and diagenetic histories related to their sensitivity to diagenetic alteration, extensive recrystallization, and complex development of their burial-stage bed dissolution or reprecipitation (Warren, 2006). Thus, geologists commonly apply isotope studies for solving these problems. The stable isotope ^{34}S stabilized approximately as +20‰ in the Earth's oceans during the whole Cenozoic (to date) together with showing oscillation during geological time (the beginning of the Mesozoic +10; the beginning of the Paleozoic +30) (Paytan et al., 2012). Marine evaporite generally follows this trend with minor fluctuations or perturbation. However, bacterial activities are taken into consideration in the evaporite environments. Palmer et al. (2004) pointed out that dissolved sulfate oxygen isotope compositions can also be affected by bacterial sulfate reduction, with the residual sulfate being enriched by between 25‰ and 50‰ (i.e. 10‰–20‰) of the enrichment in $\delta^{34}S$ (Seal et al., 2000). According to inferred data the Eğribucak evaporite facies (EGJ1, EGJ2, EGJ3) lie on the general trend for $\delta^{34}S$ of marine evaporite with a somewhat increasing rate. The enrichment of the $\delta^{34}S$ value in the evaporite of the Sivas Basin has been previously explained by bacterial sulfate reduction (Palmer et al., 2004), whereas a main drastic decrease with $\delta^{34}S$ has been observed in the single selenite crystals (F14). The diminished value of $\delta^{34}S$ would be a result of fresh-water dilution with evaporite water within the pores of the mudstone because river run-off from the continent carries lower $\delta^{34}S$ SO_4 (0‰–10‰) than seawater (Paytan et al., 2012). This conclusion related to fresh-water contribution to the marine evaporite environment is also supported by lower $\delta^{18}O$ SO_4 values in the same facies (EGJ4 and EGJ5). Except those deviations from the seawater values, EGJ1, EGJ2, and EGJ3 lie close to the contemporaneous seawater strontium and oxygen isotope curve of the Cenozoic evaporite (McKenzie et al., 1988; Denisson et al., 1998; McArthur et al., 2001), and also the $^{87}Sr/^{86}Sr$ and $\delta^{18}O$ SO_4 taken from the facies of EGJ4 and EGJ5 are nearly compatible with marine evaporite, which is also supported by previous studies based on the strontium and oxygen isotope composition of the Sivas Basin (Tekin et al., 2002; Palmer et al., 2004).

6. Discussion

6.1. Basinal configuration

Through the Eocene transgression (early to late middle Eocene) the Sivas Basin acted as an asymmetric basin that was covered by shallow-deeper marine water represented by different environments and depositional characteristics. The late Eocene regression-associated tectonic activity constrained the basin-range upliftings that divided the basin into subbasins such as Akçakışla-Düzyayla, Şarkışla-Celalli, and Akkışla-Altınyayla (Cater et al., 1991; Yılmaz and Yılmaz, 2006). The Eğribucak area was previously determined as a minibasin that resulted from salt tectonism or a diapir-bounded local basin (Ringenbach et al., 2013; Callot et al., 2014; Poisson et al., 2015; Ribes et al., 2015). Environmental and lithological correlations are very difficult to establish between these inner/minibasins due to their own depositional characters. For instance, the Akkışla-Altınyayla subbasin located in the SW of the Sivas Basin completely differs from the Eğribucak area in the east with respect to evaporite deposition and dating (Sümengen et al., 1987; Tekeli el al., 1992; Çiner and Koşun, 1996; Kangal and Varol, 1999; Çiner et al., 2002; Gündoğan et al., 2005; Yılmaz and Yılmaz, 2006) Hence, the Eğribucak area was interpreted as an isolated and very narrow inner basin within the main Cenozoic Sivas Basin, evolved from terrestrial (fluvial stage) to restricted marine (evaporite stage) and finally open marine (carbonate stage) from bottom to top.

6.2. Depositional architecture

The Eğribucak inner basin, commenced with a fluviatile deposition, underwent short-lived transgressions. These marine incursions into the terrestrial environment

Table 4. Isotopic analyses of samples recovered from the different gypsum facies of the Eğribucak section.

Sample no.	Facies	$^{87}Sr/^{86}Sr$ ‰	^{18}O ‰	^{34}S ‰
EGJ1	Bedded selenite gypsum (F10)	0.708074	11.9	23.9
EGJ2	Laminated gypsum (F11)	0.708715	11.5	23.4
EGJ3	Nodular bedded gypsum (F13)	0.708022	12.0	23.3
EGJ4	Single selenite (F14)	0.707795	4.2	10.00
EGJ5	Single selenite gypsum crystals (F14)	0.707917	4.5	10.3

constrained precipitation of nodular and enterolithic evaporite in the local sabkha environment. After pulses of marine water, the marine transgression persisted through the Oligocene. It was temporarily interrupted by short periods of regressions. Through this marine period, miliolid foraminifera-dominated carbonates were deposited in a restricted marine (lagoon) environment, temporarily inclined to evaporite-precipitated conditions that caused deposition of subaqueous bedded gypsum and single gypsum (selenite) crystals in an evaporative mudflat. These environmental fluctuations from carbonate to siliciclastic mud to evaporite suggest that the Oligocene marine water was only able to reach a sulfate concentration that was precipitated by subaqueous bedded gypsum and single diagenetic gypsum from capillary sulfate concentration within the mudstone.

6.3. Paleoenvironmental implications

The preevaporite fluvial stage is dominated by red sandstones with mud cracks and fine-grained sandy composition, widespread flood plain (red beds) and channel-fill muddy lag pebbles, and gravelly deposits and dwelling burrows, indicating a high-sinuosity-meandering river with flooding episodes (Sarkar and Chaudhuri, 1992; Kondolf and Herve, 2003; Frascati and Lanzoni, 2013). The basal fluviatiles upward graded the second siliciclastic pockets with evaporite intervening, giving an implication of environmental changes to basinal morphology and depositional characteristics. Where flood plain clastics (red beds) are diminished and replaced by coarse-grained clast-supported gravel beds, it is presumably related to a transition from a fluvial to alluvial fan depositional system that would be confirmed by the formation of some topographic elevations (Blair and McPherson, 1994; Aziz et al., 2003). The evaporite is questionable within the red-siliciclastic succession. In the study of Poisson et al. (2015) the origin of evaporites was accepted as terrestrial. Our findings are generally arguing with marine origin related to the initial phase of the Oligocene transgression towards a fluvial fan (Hayward, 1985). However, an older gypsiferous source rock, basin configuration, drainage systems, and progressive aridity would constrain the local saline environments within the fluvial fans (Arribas and Diaz-Molina, 1996). The main bedded evaporite is of marine origin, supported by strontium isotope values (Palmer et al., 2004). However, fresh-water inflows temporally diluted the evaporite environment, giving rise to wide mud deposition with single gypsum crystals (Cody and Cody, 1988). The diminished strontium isotope value of the single gypsum crystal with respect to those of the bedded gypsum is also evidence of the meteoric/fresh-water contribution into the evaporite-dominated marine environment (Paytan et al., 2012). In general, the absence of anhydrite and other salts may be attributed to low salinity brines. The abundance of the miliolid foraminifera in the evaporite-bearing carbonate unit indicates that the environment tended to be slightly brackish water, presumably occupied by a coastal lagoon. Normal marine conditions were established towards the end of the Oligocene and continued during the early Miocene, with deposited shore carbonate (platform) and offshore mud.

7. Conclusion

In spite of the Eğribucak inner basin having evolved separately as a local basin within the Sivas Basin, it provides a good environmental model affected by multistage parameters. Tectonics-salt tectonics becomes the main agent involved in the establishment of some tectonic barriers leading to environmental restriction and consequently evaporite precipitation during the maximal aridity. The Oligocene transgression was initially interrupted by short-term regressions that involved vertical and lateral environmental transitions such as siliciclastic-evaporite-carbonate in the short distances (restricted marine phase). During the end of the Oligocene, the marine transgression exceed the tectonic barriers and created the permanent marine environmental conditions (platform phase), and finally reached the maximum range (open marine phase) during the early Miocene.

Acknowledgments

The study in the Sivas Basin was financially supported by the grants to the project number ÇAYDAG-109Y041 from the Scientific and Technological Research Council of Turkey (TÜBİTAK). The authors are thankful to Serkan Akkiraz and the other anonymous reviewer for their constructive comments which helped us to improve the manuscript. We also would like to thank Sarp Tunçoku for linguistic improvement of the text.

References

Aktimur HT, Tekirli ME, Yurdakul ME (1990). Geology of the Sivas-Erzincan Tertiary Basin. Bulletin of Mineral Research and Exploration 111: 21-30.

Allan JR, Matthews RK (1982). Isotope signatures associated with early meteoric diagenesis. Sedimentology 29: 797-817.

Arribas J, Díaz-Molina M (1996). Saline deposits associated with fluvial fans, Late Oligocene-Early Miocene, Loranca Basin, Central Spain. In: Friend PF, Dabrio CJ, editors. Tertiary Basins of Spain. 1st ed. Cambridge, UK: Cambridge University Press, pp. 308-312.

Artan U, Sestini G (1971). Geology of the Beypınarı-Karababa area (Sivas Province). Bulletin of Mineral Research and Exploration 76: 80-97.

Aziz HA, Sanz-Rubio E, Calvo JP, Hilgen FJ, Krijgsman W (2003). Palaeoenvironmental reconstruction of a middle Miocene alluvial fan to cyclic shallow lacustrine depositional system in the Calatayud Basin (NE Spain). Sedimentology 50: 211-236.

Babel M (1999). History of sedimentation of the Nida Gypsum deposits (Middle Miocene, Carpathian Foredeep, southern Poland). Geol Q 43: 429-447.

Babel M (2005). Selenite-gypsum microbialite facies and sedimentary evolution of the Badenian evaporate basin of the northern Carpathian Foredeep. Acta Geol Pol 55: 187-210.

Bartholdy J, Aagaard T (2001). Storm surge effects on a back-barrier tidal flat of the Danish Wadden Sea. Geo-Mar Lett 20: 133-141.

Bathurst RGC (1966). Boring algae, micrite envelope and lithification of molluscan biosparites. Geol J 5: 15-32.

Batten Hender KL, Dix GR (2007). Facies development of a Late Ordovician mixed carbonate-siliciclastic ramp proximal to the developing Taconic orogen: Lourdes Formation, Newfoundland, Canada. Facies 54: 121-149.

Baykal F, Erentöz C (1966). 1/500.000 Ölçekli Türkiye Jeoloji Haritası, Sivas Paftası Açıklaması. MTA Ens. Yayınları. Ankara, Turkey: MTA (in Turkish).

Bingöl E (1989). Geological Map of Turkey (1:2.000.000 scale). Ankara, Turkey: Mineral Research and Exploration Institute of Turkey.

Blair TC, McPherson JG (1994). Alluvial fans and their natural distinction from rivers based on morphology, hydraulic processes, sedimentary processes, and facies assemblages. J Sediment Res 64: 450-489.

Bosence DWJ (1983). The occurrence and ecology of recent rhodoliths: a review. In: Peryt TM, editor. Coated Grains. Berlin, Germany: Springer-Verlag, pp. 225-242.

Bourquin S, Guillocheau F, Peron S (2009). Braided river within an arid alluvial plain (example from the Early Triassic, western German Basin): criteria of recognition and expression of stratigraphic cycles. Sedimentology 56: 2235-2264.

Bridge JS, Lunt IA (2006). Depositional models of braided rivers. In: Sambrook GS, editor. Braided Rivers. Ghent, Belgium: International Association of Sedimentology Special Publications, pp. 11-50.

Bull WB (1977). The alluvial fan environments. Prog Phys Geog 1: 222-270.

Callot JP, Ribes C, Kergaravat C, Bonnel C, Temiz H, Poisson A, Vrielynck B, Salel JF, Ringenbach JC (2014). Salt tectonics in the Sivas basin (Turkey): crossing salt walls and minibasins. B Soc Geol Fr 185: 33-42.

Calner M, Eriksson ME (2012). The record of microbially induced sedimentary structures (MISS) in the Swedish Palaeozoic. SEPM Special Publication 101: 29-35.

Cater JML, Hanna SS, Ries AC, Turner P (1991). Tertiary evolution of the Sivas Basin, central Turkey. Tectonophysics 195: 29-46.

Chaumillon E, Proust JN, Menier D, Weber N (2008). Incised-valley morphologies and sedimentary-fills within the inner shelf of the Bay of Biscay (France): a synthesis. J Marine Syst 72: 383-396.

Çiner A, Koşun E (1996). Stratigraphy and sedimentology of the Oligo-Miocene deposits in the south of Hafik (Sivas Basin). TAPG Bulletin 8: 16-34 (in Turkish with English abstract).

Çiner A, Koşun E, Deynoux M (2002). Fluvial, evaporitic and shallow marine facies architecture, depositional evolution and cyclicity in the Sivas Basin (Lower to Middle Miocene), Central Turkey. J Asian Earth Sci 21: 147-165.

Cody RD, Cody AM (1988). Gypsum nucleation and crystal morphology in analog saline terrestrial environments. J Sediment Petrol 58: 247-255.

Collinson JD (1986). Alluvial sediments. In: Reading HG, editor. Sedimentary Environments and Facies. 2nd ed. Oxford, UK: Blackwell Scientific Publications, pp. 20-62.

Çubuk Y (1994). Tectonostratigraphic studies on the Miocene sequences around Bogazören (Imranli) and Karayün (Hafik) (East of Sivas). PhD, Cumhuriyet University, Sivas, Turkey.

Çubuk Y, İnan S (1998). İmranlı ve Hafik güneyinde (Sivas) Miyosen havzasının stratigrafik ve tektonik özellikleri. Bulletin of Mineral Research and Exploration 120: 45-60 (in Turkish).

De Man E, Ivany L, Vandenberghe N (2004). Stable oxygen isotope record of the Eocene Oligocene transition in the southern North Sea Basin: positioning the Oil event. Neth J Geosci 83: 193-197.

Denisson RE, Kirkland DW, Evans RJ (1998). Using strontium isotopes to determine the age and origin of gypsum and anhydrite beds. J Geol 106: 1-17.

Dirik K, Güncüoğlu MC, Kozlu H (1999). Stratigraphy and pre-Miocene tectonic evolution of the southwestern part of the Sivas Basin, Central Anatolia, Turkey. Geol J 34: 303-319.

Dunham RJ (1962). Classification of carbonate rocks according to depositional textures. In: Ham WE, editor. Classification of Carbonate Rocks. AAPG Memoir. Tulsa, OK, USA: AAPG, pp. 108-121.

El-Hedeny MM (2005). Taphonomy and paleoecology of the Middle Miocene oysters from Wadi Sudr, Gulf of Suez. Revue de Paléobiologie 24: 719-733.

Filgueira R, Guyondet T, Comeau AL, Grant J (2014). Storm-induced changes in coastal geomorphology control estuarine secondary productivity. Earth's Future 2: 1-13.

Flügel E (2004). Microfacies of Carbonate Rocks. Analysis, Interpretation and Application. New York, NY, USA: Springer-Verlag.

Folk RL (1959). Practical petrographic classification of limestones. Am Assoc Petr Geol B 43: 1-38.

Folk RL (1962). Spectral subdivision of limestones types. In: WE Ham, editör. Classification of carbonate rocks. Am Assoc Petr Geol B 1: 62-84.

Frascati A, Lanzoni S (2013). A mathematical model for meandering rivers with varying width. J Geophys Res 118: 1641-1657.

Gökçe A, Ceyhan F (1988). Stratigraphy, structural features and genesis of the Miocene gypsiferous sediments in the southeastern Sivas (Turkey). Cumhuriyet University Series-A Earth Sciences 1: 91-113 (in Turkish with English abstract).

Gökçen SL, Kelling G (1985). Oligocene deposits of the Zara-Hafik region (Sivas, Central Turkey): evolution from storm-influenced shelf to evaporitic basin. Geol Rundsch 74: 139-153.

Gökten E (1983). Stratigraphy and geologic evolution of the area in the S-SE of Şarkışla (Sivas, Turkey). Bull Geol Soc Turkey 26: 167-176 (in Turkish with English abstract).

Gökten E (1993). Geology of the southern boundary of Sivas basin in the east of Ulaş Sivas-Central Anatolia): tectonic development related to the closure of Inner Tauride Ocean. TAPG Bulletin 5: 35-55.

Görür N, Oktay FY, Seymen I, Şengör AMC (1984). Paleotectonic evolution of the Tuz Gölü Basin complex, central Turkey. In: Dixon JE, Robertson AHF, editors. The Geological Evolution of the Eastern Mediterranean. London, UK: Geological Society of London Special Publications, pp. 81-96.

Guezou JC, Temiz H, Poisson A, Gürsöy H (1996). Tectonics of the Sivas Basin. The Neogene record of the Anatolian accretion along the Inner Tauride suture. Int Geol Rev 38: 901-925.

Gündoğan İ, Önal M, Depçi T (2005). Sedimentology, petrography, and diagenesis of Eocene-Oligocene evaporites: the Tuzhisar Formation, SW Sivas Basin, Turkey. J Asian Earth Sci 25: 791-803.

Hakyemez A, Özgen-Erdem N, Kangal Ö (2016). Planktonic and benthic foraminiferal biostratigraphy of the Middle Eocene-Lower Miocene successions from the Sivas Basin (Central Anatolia, Turkey). Geol Carpath 67: 21-40.

Hanford CR (1991). Marginal marine halite: sabkhas and salinas. In: Melvin JL, editor. Evaporites, Petroleum and Mineral Resources. Amsterdam, the Netherlands: Elsevier, pp. 1-66. Hayward AB (1985). Coastal alluvial fans (fan deltas) of the Gulf of Aqaba (Gulf of Eilat), Red Sea. Sediment Geol 43: 241-260.

Holliday DW (1970). The petrology of secondary gypsum rocks; a review. J Sediment Res 40: 734-744.

Hudson JD (1977). Stable isotopes and limestone lithification. Geol Soc London Memoir 133: 637-660.

Jacobsen SB, Kaufman AJ (1999). The Sr, C and O isotopic evolution of Neoproterozoic seawater. Chem Geol 161: 37-57.

Jones HL, Hajek EA (2007). Characterizing avulsion stratigraphy in ancient alluvial deposits. Sediment Geol 202: 124-137.

Kakizaki Y, Weissert H, Hasegawa T, Ishikawa T, Matsuoka J, Kano A (2013). Strontium and carbon isotope stratigraphy of the Late Jurassic shallow marine limestone in western Palaeo-Pacific, northwest Borneo. J Asian Earth Sci 73: 57-67.

Kangal Ö, Poisson A, Temiz H, Karadenizli L, Varol B, Özden S, Sirel E (2005). Sivas havzasının Eosen dönemindeki jeolojik ve sedimantolojik evrimi. Proje no: 101Y039. Ankara, Turkey: TÜBİTAK (in Turkish).

Kangal Ö, Varol B (1999). Facies of basin margin in the Lower Miocene succession of Sivas Basin. TAPG Bulletin 11: 31-53 (in Turkish with English abstract).

Kendal AC, Harwood GM (1996). Marine evaporites: arid shorelines and basins. In: Reading HG, editor. Sedimentary Environments: Processes, Facies and Stratigraphy. Oxford, UK: Blackwell Science, pp. 281-324.

Kirby MX (2000). Paleoecological differences between Tertiary and Quaternary Crassostrea oysters, as revealed by stable isotope sclerochronology. Palaios 15: 132-141.

Kondolf GM, Hervè P (2003). Tools in Fluvial Geomorphology. London, UK: John Wiley & Sons Ltd.

Kurtman F (1961). Sivas Divriği arasındaki sahanın jeolojisi ve jipsli seri hakkında müşahedeler. Bulletin of Mineral Research and Exploration 56: 1-14 (in Turkish).

Kurtman F (1973). Sivas-Hafik-Zara-İmranlı bölgesinin jeolojik ve tektonik yapısı. Bulletin of Mineral Research and Exploration 80: 1-32 (in Turkish).

Magee JW (1991). Late Quaternary lacustrine, groundwater, aeolian pedogenic gypsum in the Prungle lakes, Southeastern Australia. Palaeogeogr Palaeocl 84: 3-42.

Manzi V, Lugli S, Roveri M, Schreiber BC (2009). A new facies model for the Upper Gypsum of Sicily (Italy): chronological and paleoenvironmental constraints for the Messinian salinity crisis in the Mediterranean. Sedimentology 56: 1937-1960.

McArthur JM, Howarth RJ, Bailey TR (2001). Strontium isotope stratigraphy: Lowess Version 3: best fit to the marine Sr-isotope curve for 0–509 Ma and accompanying look-up table for deriving numerical age. J Geol 109: 155-170.

McKenzie JA, Hodell DA, Mueller PA, Mueller DW (1988). Application of strontium isotopes to late Miocene-early Pliocene stratigraphy. Geology 16: 1022-1025.

Miall AD (1978). Lithofacies types and vertical profile models in braided river deposits: A summary. In: Miall AD, editor. Fluvial Sedimentology. Calgary, Canada: Canadian Society of Petroleum Geologists, pp. 597-604.

Miall AD (1996). The Geology of Fluvial Deposits: Sedimentary Facies, Basin Analysis, and Petroleum Geology. Berlin, Germany: Springer-Verlag.

Miller KG, Feigenson MD, Wright JD, Clement BM (1991). Miocene isotope reference section, Deep Sea Drilling Project Site 608: an evaluation of isotope and biostratigraphic resolution. Paleoceanography 6: 33-52.

Milliman JD (1974). Marine Carbonates. Recent Sedimentary Carbonates Part 1. Heidelberg, German: Springer-Verlag.

Mutti M, John CM, Knoerich AC (2006). Chemostratigraphy in Miocene heterozoan carbonate settings: applications, limitations and perspectives. In: Pedley HM, Carannante G, editors. Cool-Water Carbonates: Depositional Systems and Palaeoenvironmental Controls. London, UK: Geological Society of London Special Publications, pp. 311-322.

Nebert K (1956). Zur stratigraphischen stellung der gipsserie im raum Zara-Imranli (Vilâyet Sivas). Bulletin of Mineral Research and Exploration 48: 79-85 (in German).

Ocakoğlu F (2001). Repetitive subtidal-to-coastal sabkha cycles from a Lower-Middle Miocene Marine Sequence, Eastern Sivas Basin. Turkish J Earth Sci 10: 17-34.

Okay AI, Tüysüz O (1999). Tethyan sutures of northern Turkey. Geol Soc London Special Publication 156: 475-515.

Oktay FY (1982). Stratigraphy and geological evolution of Ulukışla and its surroundings. Bull Geol Soc Turkey 25: 15-23 (in Turkish with English abstract).

Özgen-Erdem N, Kangal Ö, Varol B, Sirel E, Akkiraz S, Mayda S, Karadenizli L, Tunoglu C, Şen Ş (2013). Sivas Havzası'nın Oligosen-Miyosen Dönemi Stratigrafisi, Sedimantolojisi ve Havza Gelişimi. Proje no: 109Y041. Ankara, Turkey: TÜBİTAK (in Turkish).

Palmer MR, Helvacı C, Fallick AE (2004). Sulphur, sulphate oxygen and strontium isotope composition of Cenozoic Turkish evaporites. Chem Geol 209: 341-356.

Paytan A, Graya ET, Ma Z, Erhardt A, Faul K (2012). Application of sulphur isotopes for stratigraphic correlation. Isot Environ Healt S 48: 195-206.

Paz JDS, Rossetti DF (2006). Petrography of gypsum-bearing facies of the Codó Formation (Late Aptian), Northern Brazil. An Acad Bras Cienc 78: 557-572.

Peryt T (2008). Sedimentology of Badenian (Middle Miocene) gypsum in eastern Galicia, Podolia and Bukovina (West Ukraine). Sedimentology 43: 571-588.

Playford PE, Cockbain AE (1976). Modern algal stromatolites at Hamelin Pool, a hypersaline barred basin in Shark Bay, Western Australia. In: Walter MR, editor. Stromatolites. Amsterdam, the Netherlands: Elsevier, pp. 389-411.

Plint AG (1983). Sandy fluvial point-bar sediments from the middle Eocene of Dorset, England. In: Collinson JD, Lewin J, editors. Modern and Ancient Fluvial Systems. Oxford, UK: Blackwell Scientific Publications, pp. 355-368.

Poisson A, Guezou JC, Öztürk A, İnan S, Temiz H, Gürsoy H, Kavak KŞ, Özden S (1996). Tectonic setting and evolution of the Sivas Basin, Central Anatolia, Turkey. Int Geol Rev 38: 838-853.

Poisson A, Vrielynck B, Wernli R, Negri A, Bassetti MA, Büyükmeriç Y, Özer S, Guillou H, Kavak KS, Temiz H et al. (2015). Miocene transgression in the central and eastern parts of the Sivas Basin (Central Anatolia, Turkey) and the Cenozoic paleogeographical evolution. Int Geol Rev 105: 339-368.

Reading R (2000). Microbial carbonates: the geological record of calcified bacterial-algal mat and biofilms. Sedimentology 47: 179-214.

Reineck HE, Singh IE (1980). Depositional Sedimentary Environments. 2nd ed. New York, NY, USA: Springer-Verlag.

Reuter M, Piller WE, Brando M, Harzhauser M (2013). Correlating Mediterranean shallow water deposits with global Oligocene–Miocene stratigraphy and oceanic events. Global Planet Change 111: 226-236.

Ribes C, Kergaravat C, Bonnel C, Crumeyrolle P, Callot JP, Poisson A, Temiz H, Ringenbach JC (2015). Fluvial sedimentation in a salt-controlled mini-basin: stratal patterns and facies assemblages, Sivas basin, Turkey. Sedimentology 62: 1513-1545.

Ringenbach JC, Salel JF, Kergaravat C, Ribes C, Bonnel C, Callot JP (2013). Salt tectonics in the Sivas basin, Turkey. Outstanding seismic analogues from outcrops. First Break 31: 93-101.

Ronen A (1980). The origin of the raised pelecypod beds along the Mediterranean coast of Israel. Paleorient 6: 165-172.

Rosen MR, JK Warren (1990). The origin and significance of groundwater-seepage gypsum from Bristol Dry Lake, California, USA. Sedimentology 37: 983-996.

Sarkar S, Chaudhuri AK (1992). Trace fossils in Middle to Late Triassic fluvial redbeds, Pranhita-Godavari valley, South India. Ichnos 2: 7-19.

Schreiber BC, Freidman GM, Decima A, Schreiber E (1976). Depositional environments of upper Miocene (Messinian) evaporite deposits of the Sicilian Basin. Sedimentology 23: 729-760.

Schreiber BC, Tabakh M (2000). Deposition and early alteration of evaporites. Sedimentology 45: 215-238.

Seal RR 2nd, Rye RO, Alpers CN (2000). Stable isotope systematics of sulfate minerals. Rev Mineral Geochem 40: 541-602.

Şengör AMC, Yılmaz Y (1981). Tethyan evolution of Turkey: a plate tectonic approach. Tectonophysics 75: 181-241.

Sherman CE, Fletcher CH, Rubin KH (1999). Marine and meteoric diagenesis of Pleistocene carbonates from a nearshore submarine terrace, Oahu, Hawaii. J Sediment Res 69: 1083-1097.

Sirel E, Özgen-Erdem N, Kangal Ö (2013). Systematics and biostratigraphy of Oligocene (Rupelian-Early Chattian) foraminifera from lagoonal-very shallow water limestone in the eastern Sivas Basin (central Turkey). Geol Croat 66: 83-109.

Stchepinsky V (1939). Faune Miocene du vilayet Sivas (Turquie). Serie C, Monographie No 1. Ankara, Turkey: MTA (in French).

Stenzel HB (1971). Oysters. In: Moore RC, editor. Treatise on Invertebrate Paleontology. Part N. Mollusca 6, Bivalvia 3. Lawrence, KS, USA: Geological Society of America and University of Kansas Press, pp. N953-N1224.

Sümengen M, Terlemez I, Tayfun B, Gürbüz M, Ünay E, Özanar S, Tüfekçi K (1987). Şarkışla-Gemarek dolayı Tersiyer Havzasının stratigrafisi, sedimantolojisi ve morfolojisi. MTA Rapor No: 8118. Ankara, Turkey (in Turkish).

Sümengen M, Unay E, Sarac G, de Bruijn H, Terlemez I, Gürbüz M (1990). New rodent assemblages from Anatolia (Turkey). In: Lindsay EH, Falbusch V, Mein P, editors. European Neogene Mammal Chronology. New York, NY, USA: Plenum Press, pp. 61-72.

Tatar Y (1982). Yıldızeli (Sivas) kuzeyindeki Çamlıbel Dağlarının tektonik yapısı. Karadeniz Üniversitesi Yerbilimleri Dergisi 2: 1-20 (in Turkish).

Tekeli O, Varol B, Gökten E (1992). Sivas havzasının batı kesiminin jeolojisi (Tuzla Gölü – Tecer Dağı arası) TPAO Rapor No: 3178. Ankara, Turkey: TPAO (in Turkish).

Tekin E, Varol B, Ayan Z, Satir M (2002). Epigenetic origin of celestine deposits in the Tertiary Sivas Basin: new mineralogical and geochemical evidence. Neues Jb Miner Abh 7: 289-318.

Temiz H (1996). Tectonostratigraphy and thrust tectonics of the central and eastern parts of the Sivas Tertiary Basin, Turkey. Int Geol Rev 38: 957-971.

Testa G, Lugli S (2000). Gypsum–anhydrite transformations in Messinian evaporites of central Tuscany (Italy). Sediment Geol 130: 249-268.

Tunoğlu C, Tuncer A, Özgen N, Kangal Ö (2013). Oligocene Ostracoda from the Sivas Basin (Central Anatolia, Turkey). Naturalista Sicilia IV, XXXVII: 411-412.

Varela AN, Richiano S, Poiré DG (2011). Tsunami vs storm origin for shell bed deposits in a lagoon environment: an example from the Upper Cretaceous of southern Patagonia, Argentina. Lat Am J Sed Basin Analysis 18: 63-85.

Varol B, Atalar C (2016). Messinian evaporites in the Mesaoria Basin, North Cyprus: facies and environmental interpretations. Carbonate Evaporite (in press).

Veizer J (1983). Chemical diagenesis of carbonates: theory and application of trace element technique. In: Arthur MA, Anderson TF, Kaplan IR, Veizer J, Land LS, editors. Stable Isotopes in Sedimentary Geology 10. Tulsa, OK, USA: Society of Economic Paleontologists and Mineralogists Short Course Notes, pp. III-1-III-100.

Vermeij GJ (1972). Interspecific shore-level size gradients in intertidal molluscs. Ecology 53: 693-700.

Warren JK (1999). Evaporites: Their Evolution and Economics. Oxford, UK: Blackwell Scientific.

Warren JK (2006). Evaporites: Sediments, Resources and Hydrocarbons. Berlin, Germany: Springer.

Warren JK, Kendall CC (1985). Comparison of sequences formed in marine sabkha (subaerial) and salina (subaqueous) settings-modern and ancient. Am Assoc Petr Geol B 69: 1013-1023.

Weimer RJ, Howard JD, Lindsay DR (1982). Tidal flats. Am Assoc Petr Geol B 31: 191-246.

Wilson JL (1975). Carbonate Facies in Geologic History. Berlin, Germany: Springer.

Wright VP, Tucker ME (1991). Calciretes: an introduction. In: Wright VP, Tucker ME, editors. Calciretes. IAS Reprint Series 2. Oxford, UK: Blackwell Scientific Publications, pp. 1-22.

Yılmaz A (1981). Tokat ile Sivas arasındaki bölgede ofiyolitli karışığın içyapısı ve yerleşme yaşı. Bull Geol Soc Turkey 24: 31–36 (in Turkish with English abstract).

Yılmaz A, Yılmaz H (2006). Characteristic features and structural evolution of a post collisional basin: The Sivas Basin, Central Anatolia, Turkey. J Asian Earth Sci 27: 164-176.